2D Materials

PAPER

RECEIVED
27 March 2017

REVISED
5 June 2017

ACCEPTED FOR PUBLICATION
12 June 2017

PUBLISHED
21 July 2017

Hydrogen-induced structural transition in single layer ReS_2

M Yagmurcukardes[1], C Bacaksiz[1], R T Senger[1,3] and H Sahin[2,3]

[1] Department of Physics, Izmir Institute of Technology, 35430 Izmir, Turkey
[2] Department of Photonics, Izmir Institute of Technology, 35430 Izmir, Turkey
[3] ICTP-ECAR Eurasian Center for Advanced Research, Izmir Institute of Technology, 35430, Izmir, Turkey

E-mail: mehmetyagmurcukardes@iyte.edu.tr

Keywords: monolayer ReS_2, structural phase transition, anisotropic mechanical properties

Abstract

By performing density functional theory-based calculations, we investigate how structural, electronic and mechanical properties of single layer ReS_2 can be tuned upon hydrogenation of its surfaces. It is found that a stable, fully hydrogenated structure can be obtained by formation of strong S-H bonds. The optimized atomic structure of ReS_2H_2 is considerably different than that of the monolayer ReS_2 which has a distorted-1T phase. By performing phonon dispersion calculations, we also predict that the Re_2-dimerized 1T structure (called $\mathbf{1T}^{Re_2}$) of the ReS_2H_2 is dynamically stable. Unlike the bare ReS_2 the $\mathbf{1T}^{Re_2}$–ReS_2H_2 structure which is formed by breaking the Re_4 clusters into separated Re_2 dimers, is an indirect-gap semiconductor. Furthermore, mechanical properties of the $\mathbf{1T}^{Re_2}$ phase in terms of elastic constants, in-plane stiffness (C) and Poisson ratio (ν) are investigated. It is found that full hydrogenation not only enhances the flexibility of the single layer ReS_2 crystal but also increases anisotropy of the elastic constants.

1. Introduction

The transition metal dichalcogenides (TMDs) form a large family of layered, van der Waals-bonded materials in their bulk crystal. Isolation of monolayer TMDs leads to dramatic changes in their electronic, optical, and mechanical properties [1–4]. Following the synthesis of monolayers of Mo- and W-dichalcogenides, recently monolayers of rhenium dichalcogenides (ReS_2 and $ReSe_2$) [5] were successfully added to the TMD family. Due to their distorted structures, monolayers of ReS_2 and $ReSe_2$ exhibit anisotropic electronic, optical, and transport properties [6–8].

Similar to other TMDs, the bulk forms of Re-dichalcogenides, ReS_2 and $ReSe_2$, were reported to be in a form of van der Waals layered structure [9–11]. Raman bands and their relative intensities depending on the number of layers and the layer-stacking-order were investigated for $ReSe_2$ [12]. Recently, Yang *et al* showed that locally induced strain by generation of wrinkles in monolayer $ReSe_2$ modulates the optical gap, enhances light emission, induces magnetism, and modulates the electrical properties [13]. The structural properties of bulk ReS_2 were studied by the x-ray diffraction experiments and the symmetry properties were reported [14]. Monolayer form of ReS_2 was successfully isolated and its unique properties such as a weak band-renormalization, absence of interlayer registry and weak interlayer coupling arising from Peierls distortion of the 1T structure were reported [5]. It was also showed by Tongay *et al* that the monolayer ReS_2 has a direct band gap of 1.55 eV which was confirmed by photoluminescence measurements [5]. Pradhan *et al* investigated the field-effect transistor performance of few-layer ReS_2 [15]. They found that ReS_2 on SiO_2 behaves as an n-type semiconductor at low electron densities n. For higher values of n the resistivity decreases, and a metallic behavior is observed. Yu *et al* studied electronic properties of ReS_2 depending on applied strain and the number of layers [16]. They reported that characteristics of the band structure and its band gap are insensitive to the applied strain. Moreover, the charge carrier mobilities were found to be nearly independent of the number of ReS_2 layers. Vibrational properties, especially the low frequency modes, of ReS_2 were studied to understand coupling of ReS_2 layers. He *et al* studied the ultra low-frequency Raman spectra of ReS_2 and reported that the layers are coupled and orderly stacked in few layer ReS_2 [17]. In addition, the same analysis were reported by Lorchat *et al* in terms of the calculated force constants between ReS_2 layers [18]. The optical properties of monolayer ReS_2 were also paid much attention due to strong anisotropy in the structure [19–21]. Zhong *et al* [19] reported that the huge excitonic effects dominate the optical spectra of monolayer ReS_2 with an exciton binding energy of about 1 eV.

Tuning the physical properties of 2D materials became an important issue for their versatile use in next generation nanodevice technology. Surface functionalization of 2D monolayers with various types of atoms such as H, F, and Li, is one useful way to achieve that [22–25]. Among these atoms, H was widely used in experiments and considered also theoretically. For instance, it was first shown for graphene that hydrogenation of the sample bilaterally tunes the electronic properties significantly. Sofo *et al* predicted a form of fully saturated hydrocarbon which they named as graphane [26]. They found that the graphane is a dynamically stable material with a comparable binding energy with other hydrocarbons such as benzene and cyclohexane. Following the study of Sofo *et al*, two years later Elias *et al* successfully synthesized graphane [27] and observed that this new 2D material is an insulator. In addition, the transmission electron microscopy (TEM) measurements revealed that the graphane is a crystalline material and retains the hexagonal lattice. Moreover, it was reported that the reaction of graphene with hydrogen atoms is reversible which means graphene can be restored after annealing the graphane layer. In recent years, the hydrogenation of other novel 2D monolayers, such as TMDs, has came into prominence. Pan *et al* investigated the electronic and magnetic properties of hydrogenated monolayer VTe_2 and found that the hydrogenated VTe_2 exhibits a transition from semiconductor to metal and further to half-metal under the effect of applied tension [28]. Shi *et al* studied the electronic and magnetic properties of hydrogenated monolayer MoS_2 under applied biaxial strain and found that the ferromagnetic (FM) ground state occurs as the applied strain is increased [29].

In this study, we investigate the structural phase transition in monolayer ReS_2 by full-surface hydrogenation. The new crystal structure, $\mathbf{1T}^{Re_2}$–ReS_2H_2, is found to be dynamically stable and it is an indirect-gap semiconductor. In addition, the effect of hydrogenation on the mechanical properties is investigated. The paper is organized as follows: Details of the computational methodology are given in section 2. Structural and electronic properties of monolayers of ReS_2, single H-adsorbed ReS_2, and $\mathbf{1T}^{Re_2}$–ReS_2H_2 are presented in section 3.1. Mechanical properties of bare and hydrogenated monolayer crystals in terms of in-plane stiffness, C , effective Young modulus, E, Poisson ratio, ν, and bending rigidity, D, are presented in section 4. Finally, we conclude in section 5.

2. Computational methodology

For the first-principles calculations, we employed the plane-wave basis projector augmented wave (PAW) method in the framework of density-functional theory (DFT). The generalized gradient approximation (GGA) in the Perdew- Burke-Ernzerhof (PBE) form [30] was employed for the exchange-correlation potential as implemented in the Vienna *ab initio* simulation package (VASP) [31, 32]. The van der Waals (vdW) correction to the GGA functional was included by using the DFT-D2 method of Grimme [33]. For calculation of the band gap, effect of spin-orbit coupling (SOC) on top of GGA was considered. The charge transfer analysis was performed by using Bader technique [34].

For the electronic and geometric relaxations of the monolayer crystals, the energy cut-off value for the plane wave basis set was taken to be 500 eV. The total energy was minimized until the energy convergence becomes less than 10^{-5} eV in the structural relaxation and the convergence criteria for the total Hellmann-Feynman forces on the unitcell was taken to be 10^{-4} eV Å. To prevent possible interactions between periodic images of ReS_2 layers, a large vacuum spacing of 18 Å was considered. The minimum energy was obtained by varying the lattice constant and the pressure was reduced below 1 kbar. A Γ-centered $15 \times 15 \times 1$ k-point mesh scheme was adapted for the Brillouin zone (BZ) sampling for the primitive unit cells. The broadening for the density of state (DOS) calculations was taken to be 0.05 eV.

In order to investigate the dynamical stability of monolayers of ReS_2 and $\mathbf{1T}^{Re_2}$–ReS_2H_2, the vibrational spectra of the structures were simulated. Phonon spectra were calculated by using the small displacement method as implemented in the PHON code [35]. For the calculation of force constant matrix, 48- and 80-atom supercells were considered for monolayer ReS_2 and $\mathbf{1T}^{Re_2}$–ReS_2H_2, respectively. Each individual atom was displaced from its equilibrium position by an amount 0.04 Å in the harmonic region. In addition, we examined the stability of the monolayer ReS_2 and $\mathbf{1T}^{Re_2}$–ReS_2H_2 structures by performing *ab initio* molecular dynamic (MD) simulations.

3. Structural and electronic properties

3.1. Monolayer ReS_2

Differing from most of the TMDs having 1T or 1H phases, monolayer ReS_2 has a distorted crystal form named as 1T' phase [5] which corresponds to point group symmetry C_i. The primitive unitcell of 1T' phase is formed of eight S atoms coordinated around four-atom-cluster of Re (Re_4) as shown in figure 1(a). Our structural optimization confirms the 1T' phase of the monolayer ReS_2 as the ground state. As given in table 1, the lattice parameters a and b are found to be 6.46 and 6.38 Å, respectively. The Re–Re bond lengths in a Re_4 cluster are 2.81 and 2.71 Å for side and diagonal Re atoms, respectively. In addition, the Re–S bond length varies from 2.36 to 2.51 Å. Bader charge analysis reveals that the bond between Re and S is covalent-type with a charge depletion of 0.5 e from Re to S atom. The phonon analysis confirms that the monolayer ReS_2 is dynamically stable as shown in figure 1(b).

Electronic properties of the monolayer ReS_2 are also investigated. We find that it possesses a direct band gap of 1.45 eV calculated within GGA + SOC. As

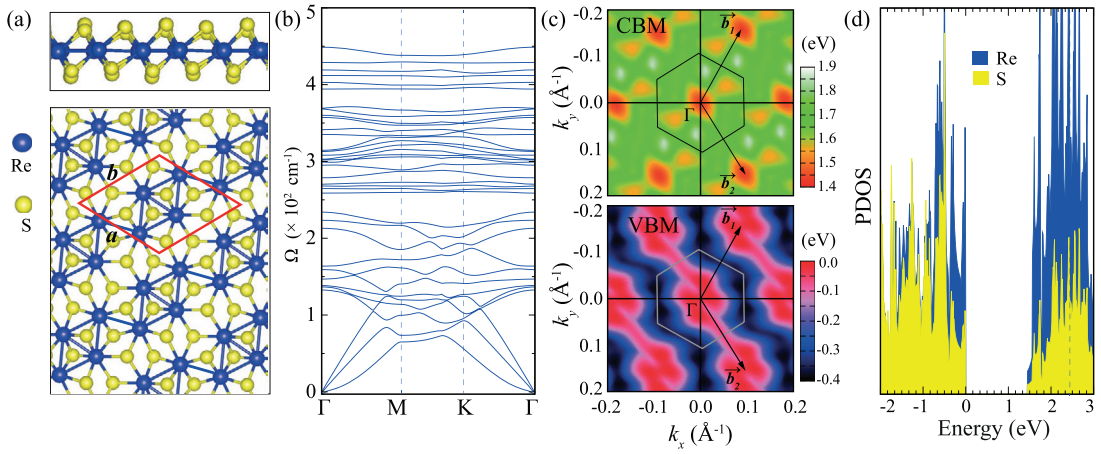

Figure 1. For the monolayer ReS_2; (a) top and side views of the structure, (b) the phonon-band structure, (c) VBM and CBM surfaces. (d) The corresponding partial density of states.

Table 1. For the monolayer ReS_2 and $1T^{Re_2}$–ReS_2H_2 structures; structure, calculated lattice parameters a and b, the average charge donation of a Re atom, $\Delta\rho$, the energy band gap of the structures calculated within; GGA (E_g^{GGA}), SOC on top of GGA (E_g^{SOC}), and the work function Φ.

	Structure	a (Å)	b (Å)	$\Delta\rho$ (e)	$E_g{}^{GGA}$ (eV)	$E_g{}^{SOC}$ (eV)	Φ (eV)
ReS_2	Re_4-cluster	6.46	6.38	0.9	1.45(d)	1.34(d)	5.56
$1T^{Re_2}$–ReS_2H_2	**Re_2-dimer**	**7.46**	**6.65**	**0.7**	**0.60**(i)	**0.75**(i)	**2.47**

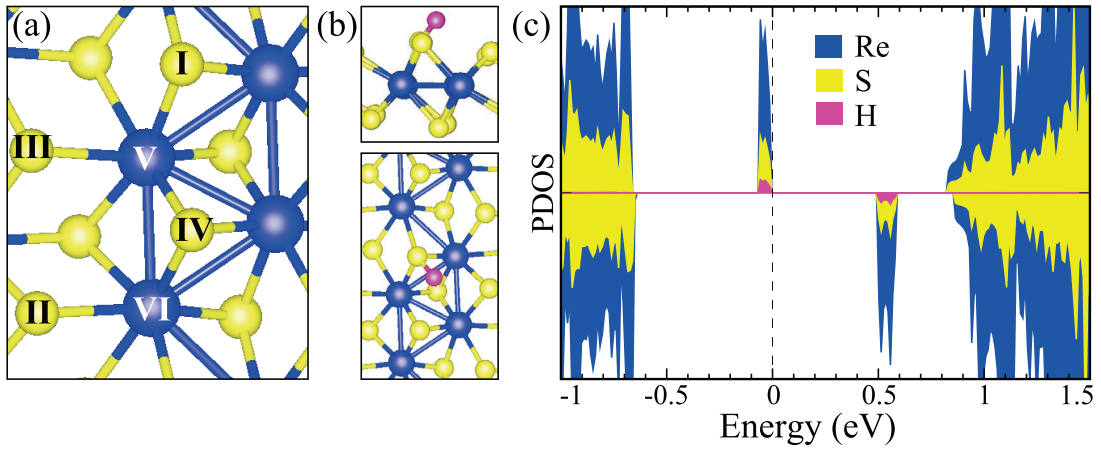

Figure 2. (a) Possible adsorption sites for a single H atom, labeled by numbers. (b) Top and side views of single H adsorbed monolayer ReS_2 and (c) the corresponding partial density of states (PDOS).

given in figure 1(c), we plot the highest of the valence band (VB) and the lowest of the conduction band (CB) energy levels as surfaces. The valence band maximum (VBM) and conduction band minimum (CBM) appear at the Γ point in BZ. The DOS calculation demonstrates that both VBM and CBM are dominated by the Re states.

3.2. Single H-atom adsorption on monolayer ReS_2

The adsorption of atoms to the surface of a material is an efficient way to tune their physical properties. For 2D materials, H atom is widely used for such purposes. In regard to functionalize the monolayer ReS_2, we first investigate the single H adsorption to the surface of the monolayer. In the unitcell, top of two Re and four S atoms are considered as the possible adsorption sites as shown in figure 2(a). Among these 6 different sites, the site-I is found to be the energetically favorable one with a S–H bond length of 1.42 Å (see figure 2(b)). The binding energy of the H atom to the surface is calculated to be 0.81 eV which is smaller than that of on graphene (0.98 eV) [36]. The single H adsorption leads to mid-gap states which appear at 0.5 eV above the VBM as shown in figure 2(c). The contributions to those mid-gap states are mainly from the Re atoms and relatively small contributions also exist from the S and H atoms. A net magnetic moment of 1 μ_B appears at the vicinity of the H bonding site.

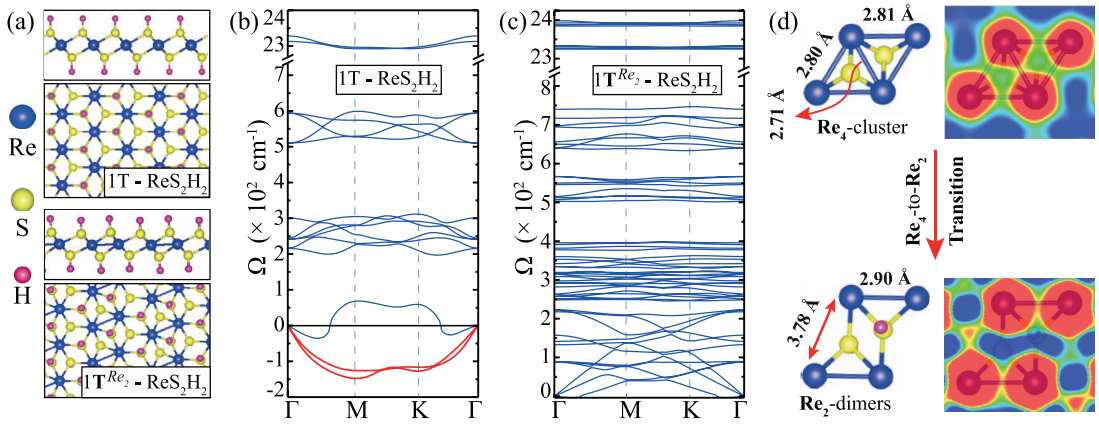

Figure 3. (a) Top and side views of monolayers of 1T-ReS_2H_2 (top panel) and **1T**^{Re_2}–ReS_2H_2 (bottom panel). Corresponding phonon-band dispersions for (b) 1T ReS_2H_2 and (c) **1T**^{Re_2}–ReS_2H_2. (d) The phase transition from Re_4 clusters in bare structure (on the left side) to Re_2 dimers in **1T**^{Re_2}–ReS_2H_2 (on the right side) and the corresponding charge densities on the same Re-planes.

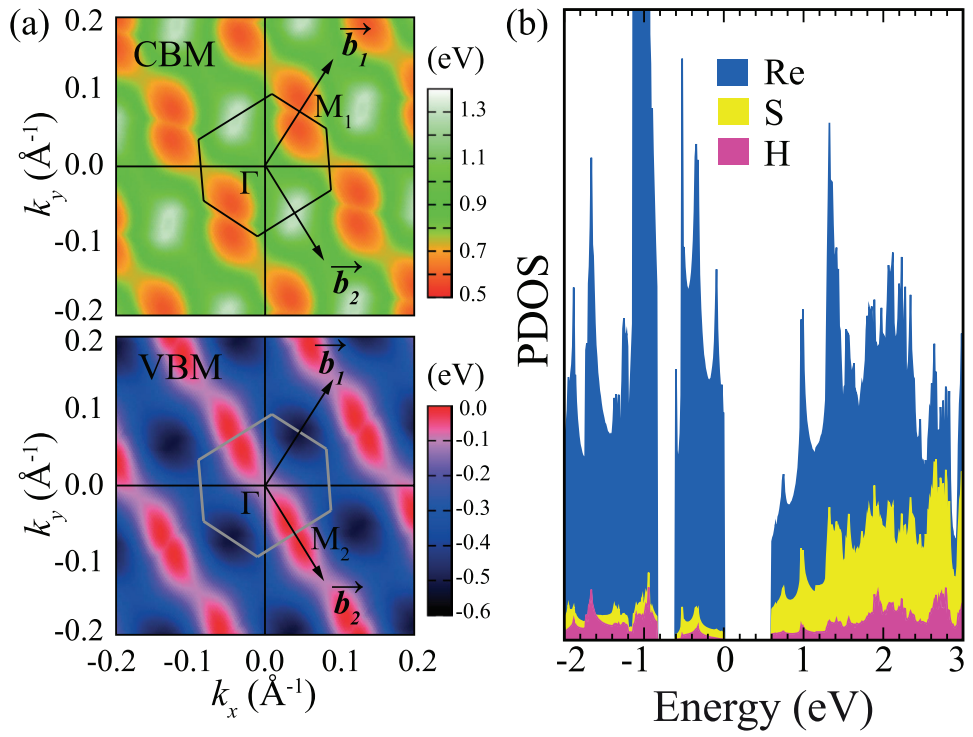

Figure 4. For the monolayer **1T**^{Re_2}–ReS_2H_2; (a) VBM and CBM surfaces and (b) the corresponding partial density of states.

3.3. Full-Hydrogenation of monolayer ReS_2

Following the analysis of the single H adsorption, we investigate the full-surface hydrogenation of the monolayer ReS_2. The full hydrogenation refers to that all the S sites are occupied by H atoms as shown in figure 3(a). The H atoms prefer to bind perpendicular to the surface plane instead of being inclined as in single H case. The full hydrogenation expands the lattice such that the parameters *a* and *b* increase to 7.46 and 6.65 Å, respectively. The most significant change in the structure is that a Re_4 cluster is broken into two Re_2 dimers as shown in figure 3(d). In this new structure which we name as **1T**^{Re_2}–ReS_2H_2, the Re–Re bond length increases to 2.90 Å, however, the Re–S bonds do not change significantly. The Bader charge analysis shows that each H atom is donated 0.1 *e* charge. In addition, the calculated phonon-band structure reveals the dynamically stability of monolayer **1T**^{Re_2}–ReS_2H_2 as shown in figure 3(c). Although, the crystal structure of monolayer **1T**^{Re_2}–ReS_2H_2 resembles the perfect 1T phase, the hydrogenated perfect 1T phase is not dynamically stable (see figure 3(b)). Thus, it is clearly seen that the formation Re_2 dimers contribute to the dynamical stability of **1T**^{Re_2}–ReS_2H_2.

The hydrogenation also modifies the electronic properties significantly. In figure 4(a), the surface plots of the VBM and CBM are shown and it is found that the **1T**^{Re_2}–ReS_2H_2 is an indirect-gap semiconductor. Its

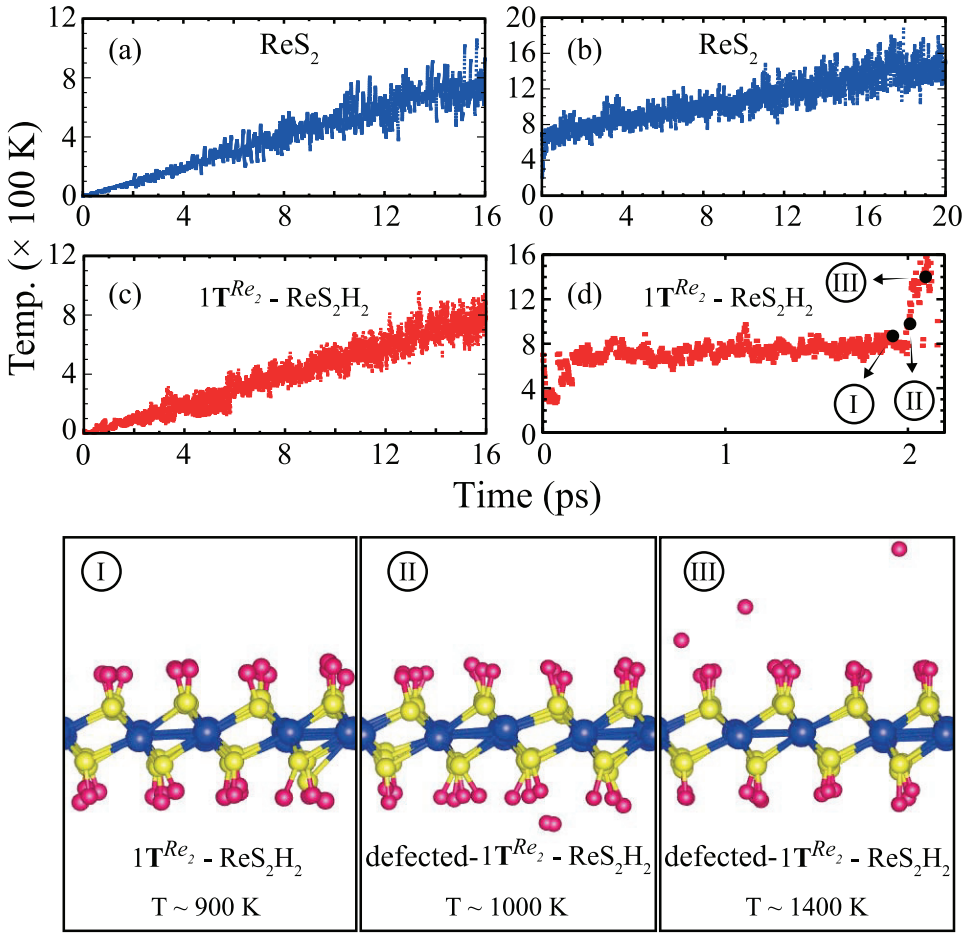

Figure 5. (Time vs. temperature diagrams of the MD simulations. Two sets of calculations are given. (a) and (c) show the first set in which the temperature increases from 0 to 800 K for the monolayer ReS_2 and **1T**^{Re_2}–ReS_2H_2, respectively. (b) and (d) show the second set in which the temperature increases from 700 to 1500 K for the monolayer ReS_2 and **1T**^{Re_2}–ReS_2H_2, respectively. (b) indicates that the monolayer ReS_2 remains stable even at 1500 K. In (d), the dissociation of the **1T**^{Re_2}–ReS_2H_2 appears as a sudden increase in the system temperature at ∼2 ps. In lower panel, the structural forms of the **1T**^{Re_2}–ReS_2H_2 are shown before and after dissociation.

band gap is 0.75 eV which is approximately half of that of monolayer ReS_2. The band extrema points do not appear at the ordinary symmetry points. The VBM of the monolayer resides between Γ and M_2 points along b_2 vector while the CBM lies between Γ and M_1 points along b_1 vector. As seen from the partial density of states (PDOS) in figure 4(b), the domination of Re states at the VBM and CBM persists.

In addition, for further examination of the stability of the monolayer ReS_2 and **1T**^{Re_2}–ReS_2H_2 structures, we perform molecular dynamics (MD) simulations under gradually increasing temperature. We consider two sets of calculations; in the first set, the temperature of each structure is increased from 0 to 800 K in a time interval of 0–16 ps, and we find that both structures remain stable as shown in figures 5(a) and (c). In the second set, the temperatures are increased from 700 to 1500 K in the time interval of 0–20 ps for each structure. For the second case, the monolayer ReS_2 remains stable (see figure 5(b)) while **1T**^{Re_2}–ReS_2H_2 dissociate after 2 ps at around 1000 K by firstly releasing the hydrogen atoms (see figure 5(d)). The corresponding structures are shown in the lower panel of figure 5.

4. Mechanical properties of monolayer ReS_2 and 1T ^{Re_2}–ReS_2H_2 Crystals

The elastic properties of 2D homogeneous monolayer materials can be represented by two independent constants, the in-plane stiffness, C, and the Poisson ratio, ν. In addition, the effective Young modulus, E, can be defined for a 2D monolayer material in terms of its proper thickness, h_p, and C to simulate its bulk behavior. In this part of the study, we analyze and discuss the mechanical properties of both of the monolayers, ReS_2 and **1T**^{Re_2}–ReS_2H_2, in terms of the elastic parameters.

The elastic constants of the monolayer ReS_2 and **1T**^{Re_2}–ReS_2H_2 are determined by using the energy-strain relation. 48- and 80-atom supercells are constructed for monolayer ReS_2 and **1T**^{Re_2}–ReS_2H_2, respectively. The supercell vectors are stretched and compressed along the ⊥ and ∥ directions, respectively. The ⊥ is defined as the perpendicular direction to Re_4 chains and ∥ is taken to be parallel to Re_4 chains. However, in the case of **1T**^{Re_2}–ReS_2H_2, these two directions are defined the same as for Re_2 dimers. The strain parameters $\varepsilon_\perp$ and $\varepsilon_\parallel$ are varied between ±0.02 with a

Table 2. Elastic parameters along ⊥- (perpendicular to Re_4 chains) and ∥-directions (parallel to Re_4 chains) for the monolayers of ReS_2 and $\mathbf{1T}^{Re_2}$–ReS_2H_2 structures; calculated in-plane stiffness $C_\perp$ and $C_\parallel$, Poisson ratio $\nu_\perp$ and $\nu_\parallel$, effective Young modulus $E_\perp$ and $E_\parallel$.

	$C_\perp$ ($J\,m^{-2}$)	$C_\parallel$ ($J\,m^{-2}$)	$\nu_\perp$ —	$\nu_\parallel$ —	$E_\perp$ (GPa)	$E_\parallel$ (GPa)
ReS_2	166	159	0.19	0.19	497	477
$\mathbf{1T}^{Re_2}$–ReS_2H_2	128	97	0.38	0.29	329	250

step size of 0.01. Then, three different sets of data are calculated; (i) $\varepsilon_\parallel = 0$ and $\varepsilon_\perp$ varying, (ii) $\varepsilon_\perp = 0$ and $\varepsilon_\parallel$ varying and (iii) $\varepsilon_\perp = \varepsilon_\parallel$ varying. At each configuration, the atomic positions are fully relaxed and the strain energy, E_S, is calculated by subtracting the total energy of the equilibrium state from the strained structure. Then, the calculated data is fitted to the equation; $E_S = c_1\varepsilon_\perp{}^2 + c_2\varepsilon_\parallel{}^2 + c_3\varepsilon_\perp\varepsilon_\parallel$ [37], and the coefficients c_i are determined.

The in-plane stiffness, C, is a measure of the rigidity of a material under applied load. Direction-dependent C can be calculated by two formulas; $C_\perp = (1/A_0)(2c_1 - c_3{}^2/2c_2)$ [39] and $C_\parallel = (1/A_0)(2c_2 - c_3{}^2/2c_1)$ [39] where $c_1 \neq c_2$ due to the anisotropy of the unit cell and A_0 is the strain-free area of the supercell. The rigidity of monolayer ReS_2 and $\mathbf{1T}^{Re_2}$–ReS_2H_2, may clearly be understood by comparing their in-plane stiffness with that of other 2D materials. Our calculated values of C are 166 and 159 $N\,m^{-1}$ for $C_\perp$ and $C_\parallel$ (see table 2), respectively for monolayer ReS_2 which are slightly different indicating very small anisotropy between these two directions. When compared with that of graphene (330 $N\,m^{-1}$ [38]) and monolayer h-BN (267 $N\,m^{-1}$ [38]), monolayer ReS_2 has a smaller C. However, due to its non-planar structure, it is meaningful to compare C of monolayer ReS_2 with that of other TMDs and other non-planar monolayers. ReS_2 is a stiff material when compared other monolayer TMDs such as MoS_2 (124 $N\,m^{-1}$) [39], $MoSe_2$ (101 $N\,m^{-1}$) [40] WS_2 (135 $N\,m^{-1}$) [41], and WSe_2 (112 $N\,m^{-1}$) [41] are considered. In addition, it is much stiffer than monolayers of GaS (91 $N\,m^{-1}$) [42] and GaSe (77 $N\,m^{-1}$) [42], non-planar monolayers of post-transition metal chalcogenide family. The rigidity of the monolayer occurs due to the covalent bonding between Re atoms in Re_4 clusters.

By the same methodology, C is calculated for monolayer $\mathbf{1T}^{Re_2}$–ReS_2H_2 and we find that $C_\perp$ and $C_\parallel$ decreases to 128 and 97 $N\,m^{-1}$, respectively. As reported for graphane (243 $N\,m^{-1}$) [43], hydrogenation reduces the value of C. In our case, the reduction in C is due to the existing of Re_2 dimers instead of Re_4 clusters in monolayer $\mathbf{1T}^{Re_2}$–ReS_2H_2. Thus, the monolayer ReS_2 becomes more flexible material upon full hydrogenation.

The Young modulus, E, is an intrinsic property of a material and generally, it is defined as the ratio of stress to the applied strain in the harmonic regime. For 2D monolayer materials an effective Young modulus can be defined in terms of h_p and C to picture out the bulk behavior of that monolayer. We calculate E by the following formula; $E = C/h_p$, where h_p is calculated from the optimized bulk structure of the monolayer.

The proper thickness of monolayer ReS_2 is calculated to be 5.95 Å and the corresponding E values are 497 and 477 GPa for $E_\perp$ and $E_\parallel$, respectively. These values are about half of that of graphite (988 GPa). In addition, these values are higher than twice of that of monolayer MoS_2 (202 GPa) [39]. Since the values of C is reduced by full hydrogenation in monolayer ReS_2, we expect the same trend for E since they are related to each other by a factor of h_p. Our geometry optimizations for the bulk form of $\mathbf{1T}^{Re_2}$–ReS_2H_2 demonstrate that the interlayer distance decreases due to the H-H interactions at the surface of $\mathbf{1T}^{Re_2}$–ReS_2H_2 layers. Thus, h_p decreases to 5.12 Å and the corresponding E values become 329 and 250 GPa for $E_\perp$ and $E_\parallel$, respectively.

The Poisson ratio is defined as the ratio of the transverse contraction strain to the longitudinal extension strain in the direction of the stretching force, that is $\nu = -\varepsilon_{trans}/\varepsilon_{axial}$. By using the parameters c_i, the Poisson ratio values along two perpendicular directions are calculated by the following formulas; $\nu_\perp = c_3/2c_2$ [39] and $\nu_\parallel = c_3/2c_1$ [39]. $\nu_\perp$ and $\nu_\parallel$ are found to be the same with a value of 0.19 for monolayer ReS_2. This value is smaller than the values reported for other monolayer TMDs (0.25 for MoS_2, 0.22 for WS_2, and 0.23 for $MoSe_2$) [41]. Generally, stiffer materials are known to posses small Poisson ratio value. Thus, reduction in C by full hydrogenation, results in the increase of $\nu_\perp$ (0.38) and $\nu_\parallel$ (0.29) for monolayer $\mathbf{1T}^{Re_2}$–ReS_2H_2. This increase in ν values demonstrates that under same longitudinal extension, the response of monolayer $\mathbf{1T}^{Re_2}$–ReS_2H_2 will be bigger than that of monolayer ReS_2.

In addition to in-plane mechanical constants, the bending rigidity which demonstrates the behavior of a monolayer material under bending deformation is of fundamental significance for applications in flexible device technology [44]. Here, the calculated bending rigidities are 9.9 and 18.2 eV for monolayer ReS_2 and $\mathbf{1T}^{Re_2}$–ReS_2H_2, respectively along ⊥ direction while 9.5 and 13.8 eV are found for ∥ direction for monolayer ReS_2 and $\mathbf{1T}^{Re_2}$–ReS_2H_2, respectively. The calculated values for monolayer ReS_2 are slightly greater than those of other monolayer TMDs such as MoS_2(6.72 eV) [45], $MoSe_2$(6.48 eV) [45], WS_2(7.60 eV) [45], and WSe_2(7.21 eV) [45]. In addition, our results indicate that although the in-plane stiffness decreases upon full hydrogenation, the bending rigidity increases due to the increase in the thickness of monolayer ReS_2 with hydrogenation.

5. Conclusion

In this study, we investigated the stability of the structure ($\mathbf{1T}^{Re_2}$–ReS_2H_2) formed upon full hydrogenation of monolayer ReS_2. Firstly, we found that single H atom can be adsorbed to the surface of monolayer ReS_2 with

a considerable binding energy (0.81 eV). Following the analysis of single H adsorption, we showed that full hydrogenation of monolayer ReS_2 results in a dynamically stable crystal structure, $\mathbf{1T}^{Re_2}$–ReS_2H_2, formed by Re_2 dimers. Our *ab initio* MD simulations demonstrated that the $\mathbf{1T}^{Re_2}$–ReS_2H_2 remains stable up to moderate temperatures, however, the hydrogen atoms dissociate at around 1000 K. Electronic-band structure calculations revealed that monolayer ReS_2 turns into an indirect-gap semiconductor upon full hydrogenation with a decreasing band gap. In addition, the analysis of elastic parameters, C, E, and ν, demonstrated that; (i) monolayer ReS_2 is a stiff material, (ii) it is not highly anisotropic in terms of elastic constants along the considered directions, and (iii) it becomes a more flexible material upon full hydrogenation. Overall, we concluded that monolayer ReS_2 can exhibit a different, dynamically stable structure upon full hydrogenation which is a flexible material suitable for nanoscale mechanical applications.

Acknowledgments

Computational resources were provided by TUBITAK ULAKBIM, High Performance and Grid Computing Center (TR-Grid e-Infrastructure). C B, H S, and R T S acknowledge the support from TUBITAK through project 114F397. H S acknowledges financial support from the Scientific and Technological Research Council of Turkey (TUBITAK) under the project number 116C073.

References

[1] Gordon R A, Yang D, Crozier E D, Jiang D T and Frindt R F 2002 *Phys. Rev.* B **65** 125407
[2] Wang Q H, Kalantar-Zadeh K, Kis A, Coleman J N and Strano M S 2012 *Nat. Nanotechnol.* **7** 699
[3] Mak K F, Lee C, Hone J, Shan J and Heinz T F 2010 *Phys. Rev. Lett.* **105** 136805
[4] Splendiani A, Sun L, Zhang Y, Li T, Kim J, Chim C Y, Galli G and Wang F 2010 *Nano Lett.* **10** 1271
[5] Tongay S *et al* 2014 *Nat. Commun.* **5** 3252
[6] Liu E *et al* 2015 *Nat. Commun.* **6** 6991
[7] Jariwala B, Voiry D, Jindal A, Chalke B A, Bapat R, Thamizhavel A, Chhowalla M, Deshmukh M and Bhattacharya A 2016 *Chem. Mater.* **28** 3352
[8] Hafeez M, Gan L, Li H, Ma Y and Zhai T 2016 *Adv. Mater.* **28** 8296
[9] Lamfers H J, Meetsma A, Wiegers G A and deBoer J L 1996 *J. Alloys Compd.* **241** 34
[10] Wildervanck J C and Jellinek F 1971 *J. Less-Common Met.* **24** 73
[11] Alcock N W and Kjekshus A 1965 *Acta Chem. Scand.* **19** 79
[12] Wolverson D, Crampin S, Kazemi A S, Ilie A and Bending S J 2014 *ACS Nano* **8** 11154
[13] Yang S *etal* 2015 *Nano Lett.* **15** 1660
[14] Wilson J A and Yoffe A D 1969 *Adv. Phys.* **18** 193
[15] Pradhan N R *et al* 2015 *Nano Lett.* **15** 8377
[16] Yu Z G, Cai Y and Zhang Y W 2015 *Sci. Rep.* **5** 13783
[17] He R, Yan J-A, Yin Z, Ye Z, Ye G, Cheng J, Li J and Lui C H 2016 *Nano Lett.* **16** 1404
[18] Lorchat E, Froehlicher G and Berciaud S 2016 *ACS Nano* **10** 2752
[19] Zhong H X, Gao S, Shi J J and Yang L 2015 *Phys. Rev.* B **92** 115438
[20] Chenet D A, Aslan O B, Huang P Y, Fan C, van der Zande A M, Heinz T F and Hone J C 2015 *Nano Lett.* **15** 5667
[21] Aslan O B, Chenet D A, van der Zande A M, Hone J C and Heinz T F 2016 *ACS Photon.* **3** 96
[22] Sahin H, Topsakal M and Ciraci S 2011 *Phys. Rev.* B **83** 115432
[23] Sahin H and Peeters F M 2013 *Phys. Rev.* B **87** 085423
[24] Cakir D, Sahin H and Peeters F M 2014 *Phys. Chem. Chem. Phys.* **16** 16771
[25] Esfahani D N, Leenaerts O, Sahin H, Partoens B and Peeters F M 2015 *J. Phys. Chem.* C **119** 10602
[26] Sofo J O, Chaudhari A S and Barber G D 2007 *Phys. Rev.* B **75** 153401
[27] Elias D C *et al* 2009 *Science* **323** 610
[28] Pan H 2014 *Sci. Rep.* **4** 7524
[29] Shi H, Pan H, Zhang Y-W and Yakobson B I 2013 *Phys. Rev.* B **88** 205305
[30] Perdew J P, Burke K and Ernzerhof M 1996 *Phys. Rev. Lett.* **77** 3865
[31] Kresse G and Hafner J 1993 *Phys. Rev.* B **47** 558
[32] Kresse G and Hafner J 1994 *Phys. Rev.* B **49** 14251
[33] Grimme S J 2006 *Comput. Chem.* **27** 1787
[34] Henkelman G, Arnaldsson A and Jonsson H 2006 *Comput. Mater. Sci.* **36** 354
[35] Alfe D 2009 *Comput. Phys. Commun.* **180** 2622
[36] Sahin H and Ciraci S 2012 *J. Phys. Chem.* C **116** 24075
[37] Nye J F 1985 *Physical Properties of Crystals* (Oxford: Clarendon)
[38] Sahin H, Cahangirov S, Topsakal M, Bekaroglu E, Akturk E, Senger R T and Ciraci S 2009 *Phys. Rev.* B **80** 155453
[39] Kang J, Sahin H and Peeters F M 2015 *Phys. Chem. Chem. Phys.* **17** 27742
[40] Kandemir A, Yapicioglu H, Kinaci A, çağin T and Sevik C 2016 *Nanotechnology* **27** 055703
[41] Guzman D M and Strachan A 2014 *J. Appl. Phys.* **115** 243701
[42] Yagmurcukardes M, Senger R T, Peeters F M and Sahin H 2016 *Phys. Rev.* B **94** 245407
[43] Topsakal M, Cahangirov S and Ciraci S 2010 *Appl. Phys. Lett.* **96** 091912
[44] Kudin K N, Scuseria G E and Yakobson B I 2001 *Phys. Rev.* B **64** 235406
[45] Lai K, Zhang W-B, Zhou F, Zeng F and Tang B-Y 2016 *J. Phys. D: Appl. Phys.* **49** 185301